The Astrophysical Journal, 655:973–979, 2007 February 1

THE ONSET OF GAMMA-RAY BURST AFTERGLOW

Shiho Kobayashi[1] and Bing Zhang[2]
Received 2006 August 5; accepted 2006 October 14

ABSTRACT

We discuss the reference time t_0 of afterglow light curves in the context of the standard internal-external shock model. The decay index of early afterglow is very sensitive to the reference time one chooses. In order to understand the nature of early afterglow, it is essential to take a correct reference time. Our simple analytic model provides a framework for understanding special relativistic effects involved in early afterglow phase. We evaluate light curves of reverse shock emission as well as those of forward shock emission, based on full hydrodynamic calculations. We show that the reference time does not shift significantly even in the thick-shell case. For external shock emission components, measuring times from the beginning of the prompt emission is a good approximation and it does not cause an early steep decay. In the thin-shell case, the energy transfer time from fireball ejecta to ambient medium typically extends to thousands of seconds. This might be related to the shallow decay phases observed in early X-ray afterglow at least for some bursts.

Subject headings: gamma rays: bursts — hydrodynamics — relativity

1. INTRODUCTION

It is well known that gamma-ray burst (GRB) afterglows decay as a power law $L \propto (t - t_0)^{-\alpha}$. The temporal decay index α, together with the spectral index, provides us precious information about GRB jets and their environment. In the pre-*Swift* era afterglow observations start typically a few hours after a burst. In such a late phase, the decay index is insensitive to the choice of the reference time t_0, and the GRB trigger time is often used in afterglow modelings.

The multiwavelength observatory *Swift* was launched in 2004 November. Thanks to its fast pointing capabilities, *Swift* is disclosing the early afterglow phase. One of unexpected finds by *Swift* is that early X-ray afterglows show a canonical behavior, in which light curves include three components: (1) a steep decay component, (2) a shallow decay component, and (3) a "normal" decay component. On top of this canonical behavior, many events have superimposed X-ray flares (Zhang et al. 2006b; Nousek et al. 2006; Chincarini et al. 2005; O'Brien et al. 2006). The transition from the early steep decay to the shallow decay typically occurs at several hundred seconds, and the timescale is comparable to the duration of rather long GRBs. When discussing the early afterglow and its connection to the prompt emission component, the decay index is very sensitive to the reference time t_0 one chooses. Correctly choosing t_0 is therefore essential to deriving the right index as well as to interpreting each component in the canonical light curve (Piro et al. 2005; Tagliaferri et al. 2005; Quimby et al. 2006).

Tagliaferri et al. (2005) investigated the first two bursts GRB 050126 and GRB 050219a, which have an X-ray light curve well sampled by the X-Ray Telescope on board *Swift*. They sought for a possible delay of the afterglow onset by fitting the early X-ray light curves (the components 1 and 2 that we have discussed above) with a single power-law model. In both cases, the decaying light curves can be fitted if the onset of the afterglow is shifted to $t_0 \sim 100$ s after the burst trigger with a single power law. However, while in the case of GRB 050126 the light curve does not allow us to clearly state whether a broken power-law modeling is better than a single power-law model, for GRB 050219a a broken power law definitively provides a better fit.

In the standard GRB model the time shift between the GRB trigger and the reference time t_0 is expected to be "small." The early steep decay should not be an artifact due to a wrong choice of t_0. Lazzati & Begelman (2006) studied forward shock emission, based on a simple energy injection model. Their numerical light curves show that measuring times from the beginning of the prompt phase is a good approximation. The early steepening and X-ray flares are likely to be produced by another mechanism (e.g., internal shocks; Burrows et al. 2005; Falcone et al. 2006; Zhang et al. 2006b; Nousek et al. 2006; Ioka et al. 2005; Fan & Wei 2005). Recently long-lasting soft emission has been reported in a short burst GRB 050724 (Barthelmy et al. 2005). Such a soft component was hinted at in the sum of multiple short BATSTE GRBs, and it might be the onset of a short burst afterglow (Lazzati et al. 2001). It is therefore of interest to quantitatively examine the t_0 issue.

In this paper, we study the physics and timescales involved in early afterglow stage, and give more direct and clear arguments for the afterglow slopes. In § 2 we study a simple analytic model. In § 3 we evaluate light curves of reverse shock emission as well as forward shock emission, based on full hydrodynamic calculations. In § 4 we address how inhomogeneity of a fireball affects an early afterglow light curve. Conclusions and discussion are given in § 5.

2. THE REFERENCE TIME t_0

Let R be a radius of a forward shock expanding with a Lorentz factor $\Gamma \gg 1$ into homogeneous ambient medium. Since the shock is moving toward us at almost the speed of light c, the difference of the observed times between a photon emitted at R and another emitted at $R + dR$ is $dt \sim dR/2c\Gamma^2$. Although the origin of observed time is arbitrary, a natural definition of observed time is given by the delay of photons emitted from a shock front at a lab time $\hat{t}$ with respect to the photons emitted from the "explosion" at $R = 0$ and $\hat{t} = 0$. The dashed line in Figure 1 depicts the trajectory of the photon from the explosion. In this paper, $\hat{t}$ and t denote the lab and observed time since the explosion, respectively.

[1] Astrophysics Research Institute, Liverpool John Moores University, Birkenhead, UK.
[2] Department of Physics, University of Nevada, Las Vegas, NV.

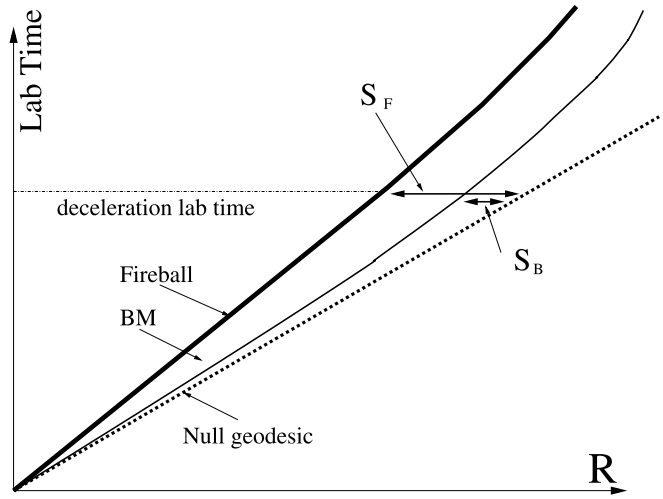

FIG. 1.—Space-time diagram; if the evolution of a fireball satisfies the BM blast wave scaling $\Gamma \propto R^{-3/2}$ from the beginning, the thin solid curve gives the trajectory. However, the fireball initially coasts with a finite Lorentz factor. The evolution is described by the BM solution only after it begins to be decelerated. At the deceleration lab time the fireball (*thick solid*) gets behind the reference BM blast wave (*thin solid*), and the trajectories approaches each other at a later time. The observed time is given by the delay of photons from an emitter at a lab time with respect to the gamma-ray front (null geodesic; *dashed line*). Null geodesics are trajectories of photons. Physical trajectories should be steeper or parallel to this minimal slope line. A trajectory of an object at rest is vertical.

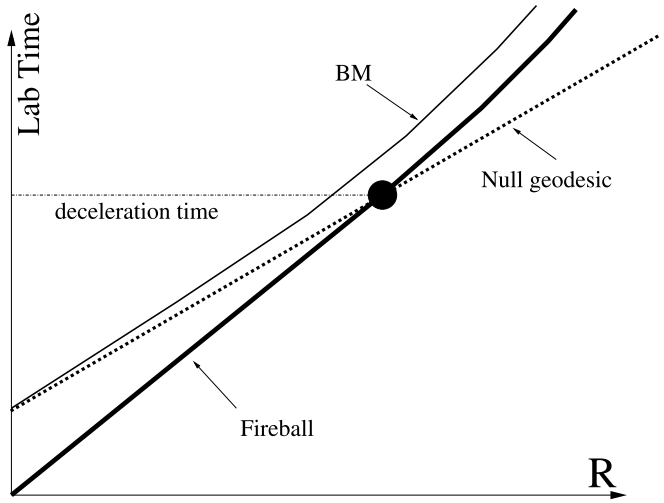

FIG. 2.—Wrong choice of t_0 : fireball evolution (*thick solid curve*), a shifted null geodesic (*dashed line*), and its reference BM blast wave (*thin solid*).

Distance, velocity, and the corresponding Lorentz factors are measured in the lab frame. Thermodynamic quantities (pressure and density) are measured in the local fluid frame. The observed time is given by

$$t = \int_0^R \frac{dR}{2c\Gamma^2}. \tag{1}$$

The shock radius is almost proportional to the lab time, $\hat{t} \sim R/c$. Considering that internal shocks occur and produce gamma rays at radii much smaller than the deceleration radius of the fireball, the prompt gamma rays associated with the outermost element of the fireball should propagate practically on the dashed line in Figure 1. The GRB trigger almost coincides with the explosion $t = 0$. The difference is small, and order of the variability timescale of the prompt emission, because the variability timescale directly reflects the inhomogeneity scale in a fireball (Kobayashi et al. 1997). The dashed line in Figure 1 will be called the gamma-ray front in the following sections.

A fireball with an initial Lorentz factor Γ_0 decelerates when it collects a large volume of ambient material with a mass density ρ_1. Equalizing energy of the shocked ambient material $4\pi R^3 \rho_1 c^2 \Gamma_0^2/3$ and fireball energy E, we obtain the deceleration radius $R_d = l/\Gamma_0^{2/3}$, where $l = (3E/4\pi\rho_1 c^2)^{1/3}$ is the Sedov length. Since the fireball density decreases as it expands, there is a possibility that a reverse shock evolves from Newtonian to relativistic during the propagation. A relativistic reverse shock considerably reduces the Lorentz factor of the fireball material which it crosses. In such a case, the energy of the shocked ambient medium is still negligible at $R = l/\Gamma_0^{3/2}$, because we have assumed $\Gamma \sim \Gamma_0$ at the deceleration to estimate R_d. The reverse shock crosses the fireball shell at $R = l^{3/4}\Delta^{1/4}$, and all the fireball material decelerates, where Δ is a fireball shell width (see Sari & Piran 1995 and Kobayashi et al. 1999 for the details). In summary, the evolution of fireballs are classified into two cases depending on the value of Δ relative to a critical value $\Delta_c = l/\Gamma_0^{8/3}$ (Sari & Piran 1995). If Δ is smaller than the critical value, it is called the thin-shell case.[3] The reverse shock is always in the Newtonian regime, and it is too weak to slow down the fireball effectively. The deceleration radius is $R_d = l/\Gamma_0^{2/3}$. If $\Delta > l/\Gamma_0^{8/3}$ (the thick-shell case), we define the deceleration radius as the shock crossing radius $R_d = l^{3/4}\Delta^{1/4}$. The deceleration lab time is given by $\hat{t}_d \sim R_d/c$.

If the Blandford-McKee (BM) blast wave scaling $\Gamma \propto R^{-3/2}$ (Blandford & McKee 1976) was valid for the whole fireball evolution (Fig. 1, *thin solid line*), integrating equation (1), we obtain $R \propto t^{1/4}$. Since the spectral characteristics of forward shock synchrotron emission are given by products of t, $R(t)$, $\Gamma(t)$, and constant parameters (Sari et al. 1998), the light curve should be described by a power law with the reference time $t_0 = 0$. However, the BM blast wave scaling is applicable only after the fireball is decelerated (e.g., Kobayashi et al. 1999). At earlier times the fireball (*thick solid line*) is in the coasting phase, and it is slower than evaluated from the BM blast wave scaling. The delay of photons from the shock front at the deceleration lab time is larger by $\delta t = (S_F - S_B)/c$ than in the case that the BM blast wave scaling is applicable to the whole evolution (see Fig. 1), where S_B and S_F are the separations at the deceleration lab time between the gamma-ray front (*dashed line*) and the reference BM blast wave (*thin solid line*), and between the gamma-ray front and the fireball forward shock (*thick solid line*), respectively. The reference time for the afterglow modeling is given by

$$t_0 \equiv \frac{S_F - S_B}{c}. \tag{2}$$

In the thick-shell case, a forward shock keeps being energized for a longer time, and the deceleration phase starts at a later time. It still overestimates the shift of the reference time if t_0 is set at the end of the energy injection or equivalently at the peak time of afterglow. In Figure 2 the dot indicates the point at which the energy injection stops and the fireball turns into a BM solution. Measuring times from the peak of afterglow corresponds

[3] In the thin-shell case, the deceleration observed time is given roughly by the critical width $\sim \Delta_c/c = R_d/c\Gamma_0^2$, and it is longer than the duration of the prompt emission Δ/c (Sari 1997). The deceleration time Δ_c/c approaches Δ/c if we take a larger Γ_0, and around $\Gamma_0 \sim \Gamma_c = (l/\Delta)^{3/8}$ (or equivalently $\Delta \sim \Delta_c$) a reverse shock becomes relativistic during the propagation. The Lorentz factor of the shocked material at the crossing time becomes independent from the initial value, and it is given by Γ_c. The deceleration observed time is about $R_d/c\Gamma_c^2 = \Delta/c$.

to defining a reference null geodesic (*dashed line*) as it goes through the dot. Imagine the reference BM blast wave (*thin solid line*) associated with the new reference null geodesic.[4] The decay of the emission from this reference blast wave should be characterized by a power law using the new reference time (measuring times from the peak). The evolution of a real fireball (*thick solid line*) is also described by a BM blast wave after the deceleration. However, it is a different solution (a different curve on the diagram). Applying the new reference time to the afterglow modeling leads to a wrong estimate of the decay index, especially in the early phase. The decay index should become shallower than the real value.

Using equation (1) and the evolution of a BM blast wave $\Gamma \sim (R/l)^{-3/2}$, we obtain $S_B = R_d/8\Gamma_d^2$, where Γ_d is the Lorentz factor at the deceleration radius R_d. Since the Lorentz factor of a fireball is constant $\Gamma = \Gamma_0$ at $R < R_d$, we get $S_F = 4S_B$ for the thin shell. In the thick-shell case, a reverse shock becomes relativistic before it crosses the fireball shell, and it begins to reduce considerably the Lorentz factor of the shell's matter which it crosses. The Lorentz factor of the forward shock is also significantly reduced as $\Gamma \sim (l^3/\Delta R^2)^{1/4}$ during the reverse shock crossing (Sari & Piran 1995; Kobayashi et al. 1999), and we get $S_F = 2S_B$ for the thick shell. The reference time is given by

$$t_0 = t_d\left(1 - \frac{S_B}{S_F}\right) = \begin{cases} 3t_d/4 & \text{thin shell case,} \\ t_d/2 & \text{thick shell case,} \end{cases} \quad (3)$$

where $t_d = S_F/c$ is the deceleration observed time.

We have considered a simple broken power-law model for the evolution of a fireball Lorentz factor, and we obtained equation (3). In reality the fireball should decelerate gradually around the deceleration radius. An artificial early steepening could happen only when $S_B \ll S_F$, and in such a case t_0 should be set at t_d (the afterglow peak time) to get the correct α. However, in both the thin shell and thick-shell cases, we have found that S_B and S_F are comparable. Therefore, measuring times from the beginning of the prompt phase $t_0 = 0$ should not induce an overestimate of afterglow decay right after the peak.

Equation (1) gives the delay of photons emitted from a point on the shock front on the line of sight, while most photons suffer longer delays, since they are emitted from a shocked region of finite thickness behind the shock, and from positions off the line of sight. Although these effects could make both separations S_B and S_F larger by a factor of a few (Waxman 1997), they are still comparable and our arguments are valid.

3. NUMERICAL MODEL

We employ a spherical relativistic Lagrangian code based on the Godunov method with an exact Riemann solver to evaluate the hydrodynamic evolution of a relativistic fireball (Kobayashi et al. 1999; Kobayashi & Sari 2000). Using the Einstein summation convention the equations describing the motion of a relativistic fluid are given by the five conservation laws

$$\partial(\rho u^i)/\partial x^i = 0, \ \partial T^{ik}/\partial x^k = 0, \quad (4)$$

where u^i is four velocity and T^{ik} is the stress-energy tensor $(i, k = 0, \ldots, 3)$, which for a perfect fluid can be written as $T^{ik} = wu^iu^k - pg^{ik}$. Here g^{ik} is the metric tensor, p is the fluid pressure, and $w = e + p$ is the heat function per unit volume. Shocked material is extremely hot, and pressure is related to internal energy e and mass density ρ as $p = (e - \rho c^2)/3$. In the Godunov scheme, conservative variables are considered as piecewise constants over the mesh cells at each time step, and the time evolution is determined by the solution of the Riemann problem (shock tube) at the intercell boundaries (e.g., Martí & Müller 1999, and references therein).

Because of the relativistic beaming effect, the radiation from a jet before the jet break can be described by a spherical model with an isotropic energy. The initial configuration for our simulation is a static uniform fireball surrounded by uniform cold ambient material (ISM). It is determined by four parameters: an isotropic energy E, a dimensionless entropy Γ_0, an initial radius R_0, and the ISM mass density ρ_1. The terms E and ρ_1 always appear as the ratio E/ρ_1 in the hydrodynamics computation, so the system is actually determined by three parameters, the initial radius R_0, the entropy Γ_0, and the Sedov length l. For convenience, we set the initial lab time as R_0/c rather than zero in numerical calculations, and the observed time is determined by the delay of photons from an emitter with respect to the photons emitted from the initial fireball surface at $R = R_0$ and $\hat{t} = R_0/c$. Since the fireball immediately accelerates to a relativistic velocity, this is practically equivalent to the observed time used in Figure 1.

We carry out numerical calculations for the total number of mesh cells $N = 540$.[5] A third of the cells are for the fireball, while the other cells describe the ambient medium within $R_{\max} = 10^{18}$ cm. Although the initial configuration is $\sim$55 cells per decade, the nature of Lagrangian method gives a much higher resolution for shocks, which sweeps cells and compresses them by a factor of $\sim\Gamma^2$. A reflection boundary and free boundary condition are imposed at the center $R = 0$ and at $R_{\max}$, respectively. We consider two cases, the thin- and thick-shell.

3.1. *The Thin-Shell Case*

We first consider the thin-shell case: $E = 10^{53}$ ergs, $\Gamma_0 = 100$, $R_0 = 3 \times 10^{11}$ cm, and $\rho_1 = 1\ m_p\ \mathrm{cm}^{-3}$ where m_p is the proton mass. Initially, as the fireball expands into a surrounding medium, a narrow shell with a radial width $\Delta \sim R_0$ is formed. The Lorentz factor of the shell increases linearly with the radius during the free acceleration stage. Then, the fireball shell uses up all its internal energy, and it coasts with the Lorentz factor of Γ_0. The coasting ends once the ISM begins to influence the shell. After the deceleration radius R_d, the profile of the shocked ISM medium begins to approach the BM solution. The evolution of a fireball is fully discussed by Kobayashi et al. (1999).

The interaction between the shell and the ISM is described by two shocks: a forward shock propagating into the ISM and a reverse shock propagating into the shell. Figure 3 shows the propagation of the shocks. Initially, the unshocked fireball shell has all the energy of the system. As the shell expands, the reverse shock decelerates the ejecta while the forward shock accelerates the ISM. The energy is transferred from the unshocked shell to the ISM via the shocks, finally the shocked ISM carries essentially all the energy of the system. In the intermediate stage, around the deceleration time $t_d = (3E/32\pi\rho_1 c^5\Gamma_0^8)^{1/3} \sim 195$ s, the shocked shell has comparable energy to the shocked ISM. The evolution of the energies in three regions, inside of the reverse shock (unshocked shell), between the reverse shock and the contact

[4] BM blast wave lines on the space-time diagram are determined by two parameters, an explosion time (i.e., a null geodesic on the diagram) and the Sedov length. The latter is evaluated with the total fireball energy if there is energy injection before the deceleration time.

[5] We have reevaluated the light curves Figs. 5 and 7 for $N = 5400$. In the log-log space, the resulting light curves are almost identical. The differences are less than several percent. When we remove numerical oscillations, they are in a few percent agreement.

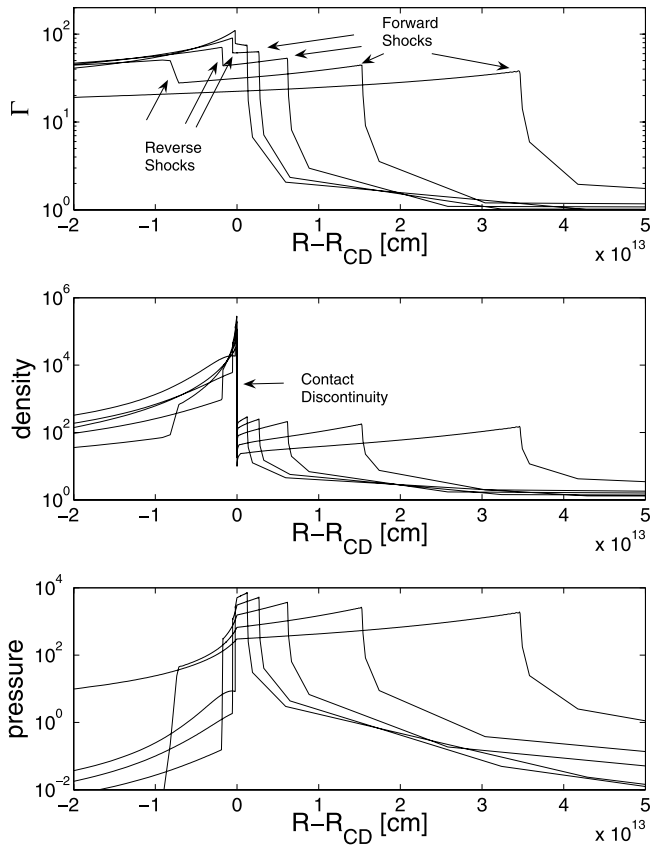

FIG. 3.—Thin-shell case: profiles of Γ, ρ, and p at different lab times $\hat{t} = 0.62R_d/c, 0.86R_d/c, 1.14R_d/c, 1.45R_d/c$, and $1.74R_d/c$. The x-axis is the distance from the contact discontinuity (CD). Photons emitted from the discontinuity at the lab times are observed at $t = 100, 200, 400, 840$, and 1650 s, respectively. The gamma-ray front is located at $(R - R_{\rm CD}) = ct$.

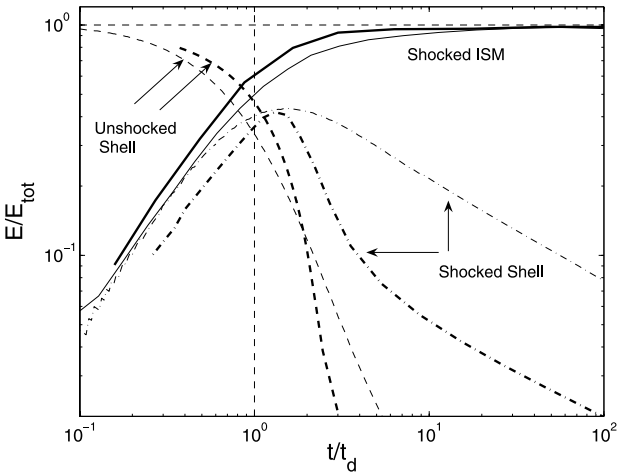

FIG. 4.—Energy transfer from the fireball to the shocked regions for the thin-shell case (*thin lines*) and the thick-shell case (*thick lines*). The sum of the kinetic energy and the thermal energies are also shown in the unshocked shell (*dashed lines*), in the reverse shocked shell (*dashed-dotted lines*) and in the forward shocked ISM (*solid lines*). All the energies are normalized by the explosion energies. The observed time is normalized by the deceleration time t_d.

discontinuity (shocked shell), and between the contact discontinuity and the forward shock (shocked ISM) are shown in Figure 4. The observed times of photons from the reverse shock front; the contact discontinuity and the forward shock front are used to describe the evolution of the energies.

Even after the deceleration time, the reverse shocked shell (Fig. 4, *thin dashed-dotted line*) carries a significant fraction of the system energy for a long time, 20% at $t \sim 10t_d$ and 10% at $t \sim 45t_d$. In the thin-shell case, the reverse shock is Newtonian, or subrelativistic in the frame of the unshocked shell (the deceleration by the reverse shock is not significant as we can see in the top panel of Fig. 3). It does not heat the shocked region well. The reverse shocked region is already cold at the shock crossing time (the deceleration time), and the shocked shell carries the energy mainly in the form of the kinetic energy $E \propto \Gamma$. Assuming a power-law decay $\Gamma \propto R^{-g}$, we obtain $E \propto \Gamma \propto t^{-g/(1+2g)} \sim t^{-0.4}$ for $g = 2.2$ (Kobayashi & Sari 2000).

This slow energy transfer should lead to the round-off of an afterglow peak. To evaluate the afterglow light curve, we consider here a simple case in which the energy of the magnetic field remains a constant fraction of the internal energy $B^2 \propto p$. The electron random Lorentz factor evolves as $\gamma_m \propto p/\rho$ after the shock heating, where p and ρ are the pressure and density of a fluid element, respectively. The typical synchrotron frequency in the observer frame is $\nu_m \propto \Gamma\gamma_m^2 B$. Since a relativistic shock totally ionizes material that it crosses, the total number of electrons in a fluid element (mesh cell) is $N_e = 4\pi R^2 dR\Gamma\rho/m_p$, where dR is a cell width in the lab frame. The spectral power at the typical frequency from a cell is given by $F_{\nu_m} \propto N_e\Gamma B$. Assuming a power-law distribution of the electron random Lorentz factor with index $\hat{p}$, the observed flux is

$$F_{\nu_m<\nu<\nu_c} = F_{\nu_m}\left(\frac{\nu}{\nu_m}\right)^{-(\hat{p}-1)/2} \propto N_e\Gamma^{(\hat{p}+1)/2}p^{(5\hat{p}-3)/4}\rho^{-(\hat{p}-1)}, \quad (5)$$

where we have assumed that the observational band is located between the typical frequency ν_m and the cooling frequency ν_c. In early afterglow phase, with the typical parameters, the X-ray and optical bands satisfy this condition for the forward shock and reverse shock emission, respectively.[6] We evaluate the flux and observed time of photons from each shocked fluid element, and superimpose the emission to construct the forward and reverse shock light curves. The results are shown in Figure 5. Although at later times the light curves approach the expected power law decays $L \propto t^{-1}$ (forward shock; *thick solid line*) and $L \propto t^{-2}$ (reverse shock; *thin solid line*), the peaks are rounded as we expected.

At the deceleration time (and after that), the light crossing time of the forward shocked region is comparable to the observed time $\Delta/c \sim R/c\Gamma^2$. To evaluate the effect of the thickness of the forward shocked region, we assume that all the shocked electrons emit photons at the forward shock front. The resulting light curve peaks at an earlier time $t \sim t_d/2$,[7] but the shape around the peak itself is similar. We conclude that the round-off of the afterglow

[6] For the typical microscopic parameters $\epsilon_e = 10^{-2}$ and $\epsilon_B = 10^{-3}$, the numerical results shown in this paper actually satisfy this condition in the time ranges of the plots (Figs. 5 and 7), where ϵ_e and ϵ_B are the fractions of shock energy given to magnetic field and electrons at a shock, respectively. Choosing a larger ϵ_B could produce an additional break at $t \sim 10^3$–10^4 s especially in X-ray light curves due to the passage of the forward-shock cooling frequency in X-ray band. However, the steepening is small $\Delta\alpha = 1/4$, and it happens well after the deceleration of the fireball. The cooling break does not affect our discussions about the onset of afterglows.

[7] A peak time is given by the sum of a deceleration time and a fraction of the light crossing time of a shocked region. If all the shock energy is assumed to be radiated at the shock front, the emission should peak earlier. The analytic deceleration time t_d is obtained based on a simple model, and it could have an error of a factor of a few.

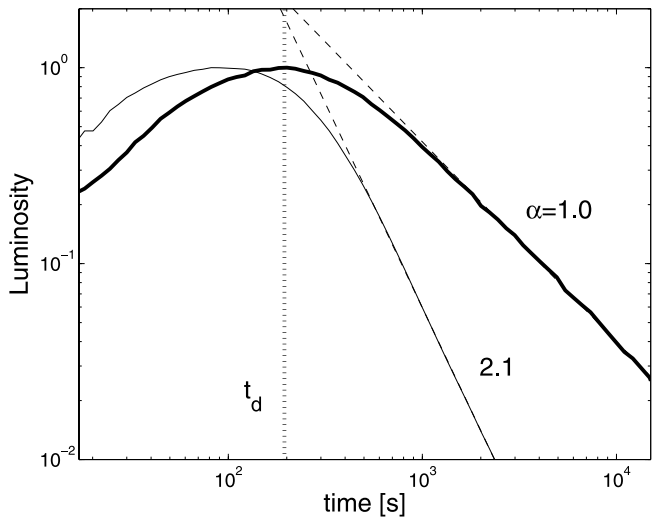

FIG. 5.—Afterglow light curve for the thin-shell case here; $E = 10^{53}$ ergs, $\Gamma_0 = 100$, $R_0 = 3 \times 10^{11}$ cm, $\rho_1 = 1 m_p$ cm^{-3}, and $\hat{p} = 2.2$. Forward shock emission in X-ray band (*thick curve*) and reverse shock emission in optical band (*thin curve*) and power-law fits (*dashed lines*) for the forward shock $\alpha = 1.0$ and reverse shock $\alpha = 2.1$ are also shown. The light curves are normalized at the peaks.

peak is mainly due to the slow energy transfer from a fireball shell to a blast wave.

The internal shock model requires a highly irregular outflow from the GRB central engine. Since the hydrodynamic interaction inside the flow smooths the velocity and pressure profiles, but not the density profile, fireball ejecta might have an irregular density profile at the deceleration time. Emission from the ejecta during a reverse shock crossing could reflect the light curve of the prompt emission produced by internal shocks (Nakar & Piran 2004). The peak time of the reverse shock emission also depends on the density profile. As a fireball expands, a reverse shock accelerates more and more electrons in the fireball, while the Lorentz factor and pressure of the shocked region decreases. The balance determines the peak time. In the thin-shell case, a reverse shock does not effectively decelerate the shell material that it crosses. This leads to large pressure gradient across the shocked region. The contribution of emission from the inner part of the shell becomes negligible, and the reverse shock emission peaks slightly before the shock crossing time (*thin solid line*).

3.2. *The Thick-Shell Case*

We consider the thick-shell case in which a reverse shock becomes relativistic during the propagation. The initial condition is $E = 10^{52}$ ergs, $\Gamma_0 = 10^3$, $R_0 = 3 \times 10^{11}$ cm, and $\rho_1 = 10 m_p$ cm^{-3}. The fireball is decelerated around $R_d = l^{3/4} R_0^{1/4} \sim 1.5 \times 10^{16}$ cm, which corresponds to the shock crossing time $t_d = R_0/c = 10$ s.

The energy transfer from the fireball to a blast wave is similar to that described in the thin-shell case. At the shock crossing time, the forward-shocked ISM and reverse-shocked shell have comparable energies (*thick lines*, Fig. 4). The main difference is that in the thick-shell case the shocked shell carries the energy in the form of the internal energy, instead of the kinetic energy, because the reverse shock significantly decelerate the shell. Figure 6 depicts the profiles of Γ, ρ, and p. When the reverse shock crosses the shell with a width of $\sim R_0$, a rarefaction wave begins to propagate toward the contact discontinuity, and it quickly transfers the shell's internal energy to the shocked ISM in a timescale comparable to the deceleration time (the shock crossing time). The

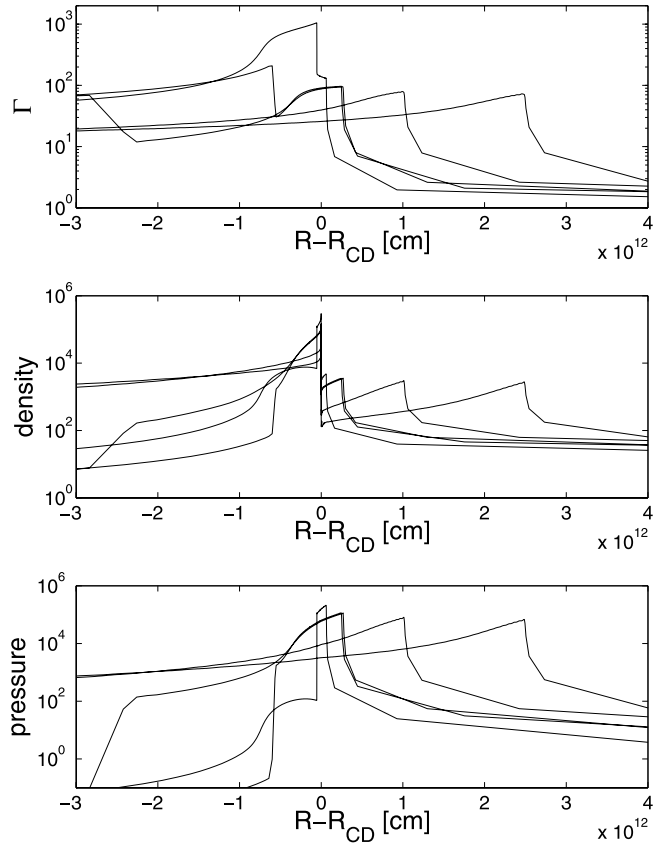

FIG. 6.—Thick-shell case, showing profiles of Γ, ρ, and p at different lab times $\hat{t} = 0.75 R_d/c$, $1.40 R_d/c$, $1.45 R_d/c$, $1.92 R_d/c$, and $2.14 R_d/c$. The x-axis is the distance from the contact discontinuity (CD). Photons emitted from the discontinuity at the lab times are observed at $t = 5, 18, 19, 50$, and 100 s, respectively. The gamma-ray front is located at $(R - R_{\rm CD}) = ct$.

steep decay of the shocked shell energy right after the peak (*thick dashed-dotted line*) is due to the rarefaction wave propagation. Since for our parameters the reverse shock is mildly relativistic in the frame of the unshocked shell $\tilde{\Gamma} \sim \Gamma_0/(l/R_0)^{3/8} \sim$ several (Sari & Piran 1995), the shocked shell becomes cold after the propagation, and the energy of the shocked shell begins to decay in the same rate as the thin shell does.

In the thick-shell case, the energy of a shocked shell is swiftly relayed to a forward shock by a rarefaction wave. A broken power law $\Gamma \propto R^{-1/2} (R < R_d)$ and $\Gamma \propto R^{-3/2} (R > R_d)$ describes the evolution of the forward shock well. The round-off of an afterglow peak is expected to be small. Using equation (5) and numerical results, we evaluate the light curves of the forward shock and reverse shock emission, which are shown in Figure 7. Initially the luminosity of the both shocked region slowly increases as $\sim t^{1/2}$ (Kobayashi 2000), and they peak around the shock crossing time. The forward shock light curve (*thick solid curve*) is slightly steeper right after the peak compared to at late times. Although the decay is described well by a single power law if the reference time t_0 is set at the middle between the GRB trigger and the afterglow peak as we discussed in § 2, measuring times from the GRB trigger also provides a reasonable estimate for the afterglow decay. The reverse shock emission (*thick dashed curve*) drops sharply $\alpha \sim 5$ during the rarefaction wave propagation. The high-latitude (off-axis) emission could contribute to the early flux (Kumar & Panaitescu 2000). The numerical fireball shell has a long tail in the density profile, and the shocked tail contributes to the light curve at late times. The emission from the outer part

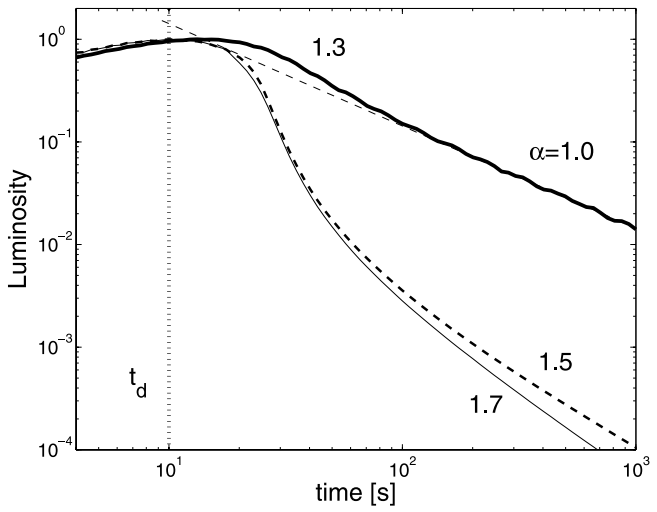

FIG. 7.—Afterglow light curve for the thick-shell case; $E = 10^{52}$ ergs, $\Gamma_0 = 1000$, $R_0 = 3 \times 10^{11}$ cm, $\rho_1 = 10 m_p$ cm^{-3}, and $\hat{p} = 2.2$. Forward shock emission in X-ray band (*thick solid curve*) and reverse shock emission in optical band (*thick dashed curve*) are also shown. Reverse shock emission from the outer part of the shell corresponds to 80% of the shell mass (*thin solid curve*). Forward shock emission decays slightly faster at the beginning as $t^{-1.3}$ and later it decays as $t^{-1.0}$; reverse shock decay indexes as $\alpha = 1.5$ and $\alpha = 1.7$. The deceleration time $t_d = R_0/c = 10$ s (*vertical dotted line*). The light curves are normalized at the peaks.

containing 80% of the shell mass gives a steeper light curve (*thin solid curve*).

4. INHOMOGENEOUS FIREBALL

If a burst has a precursor, we might need a shift of the reference time to a later time. A simple example is that a precursor with a negligible energy is followed by the main component. The quiescent period could be due to a dormant period in the central engine or to the property of the outflow (e.g., homogeneous outflow in which prompt gamma rays are not produced by internal shocks). In the former case, t_0 should be set at the explosion time of the main component. If the separation between the precursor and the main component is much larger than the deceleration time of the main component, measuring times from the precursor introduces an artificial steeping in the early afterglow. Assuming a precursor and measuring times from it, we have replotted Figures 5 and 7. If the precursor is located at $\Delta t \sim 2000$ s $\sim 10 t_d$ or ~ 3500 s $\sim 18 t_d$ before the main component, the decay index of the early forward shock emission could be overestimated as $\alpha \sim 3$ or ~ 5 in the thin-shell case. In the thick-shell case, $\Delta t = 7 t_d$ and $12 t_d$ lead to steep decay indexes of $\alpha \sim 3$ and ~ 5, respectively. Since afterglow light curves are usually plotted with t_0 at the GRB trigger time, precursors, although they might be energetically small, need to be strong enough to trigger GRB detectors (e.g., BAT) in order to cause an artificial steep decay.

4.1. *Case Studies*

X-ray flares were originally reported from *BeppoSAX* observations, GRB 011121 and GRB 011211 (Piro et al. 2005). GRB 011121 was the second-brightest GRB observed by *BeppoSAX* in gamma rays (after GRB 990123) and in X-rays (after GRB 010222). The fluence in the 2–700 keV range corresponds to an isotropic energy of 2.8×10^{52} ergs at the redshift of the burst $z = 0.36$. The gamma-ray light curve shows a main peak starting at $t \sim 5$ s and ending at $t \sim 30$ s with minor substructures. An X-ray flare took place at $t = 240$–310 s. The fluence of GRB 011211 in the 2–700 keV range gives an isotropic energy of 3.6×10^{52} ergs at the redshift of the burst $z = 2.14$. The gamma-ray prompt emission has a long duration $T \sim 400$ s, and an X-ray flare is detected from 600 to 700 s. In the source frame, the two flares occurred at a similar time ~ 200 s and they have a width $\Delta/c \sim 30$–50 s (see Piro et al. 2005 and references therein for the basic parameters of these bursts).

Since the decay part of the X-ray flares and the following shallower part are described with a single power law when the time is measured starting from the flare peak, the flares were suggested as the beginning of the afterglow caused by a thick shell (Piro et al. 2005). The thick-shell interpretation requires a long energy release from the central engine. The burst should be long and extend all the way to the flare peak. However, the observed prompt emission ended well before the onset of the flares. In order to suggest the thick-shell case, one must assume that the efficiency of conversion into gamma ray varies dramatically with time. Furthermore, the engine should release most fireball energy at the last moment (major reenergization at the flare), because measuring times from the GRB trigger does not lead to an overestimate of the decay index even in the thick-shell case, as long as the shell is homogeneous.

In principle, the low conversion efficiency could originate from: (1) a small Lorentz factor of late ejecta, which does not allow gamma-ray radiation; or (2) a small dispersion of the Lorentz factor of late ejecta in the internal shock scenario. The critical Lorentz factor is given by $\Gamma_c = (3E/4\pi\rho_1 c^2 \Delta^3)^{1/8} \sim 310 E_{53}^{1/8} \rho_{1,-1}^{-1/8} \Delta_{12}^{-3/8}$ where $Q_n = Q/10^n$ is in cgs units and $\Delta_{12} \sim \Delta/(c \times 40\ \mathrm{s})$. In scenario 1, the low Lorentz factor condition $\Gamma \lesssim 100$ requires that the last energetic ejecta with an energy $E \gtrsim 10^{53}$ ergs and a width $\Delta/c \sim 40$ s should be in the thin-shell regime. The deceleration observed time $t_d \gtrsim 420 E_{53}^{1/3} \rho_{1,-1}^{-1/3} \Gamma_2^{-8/3}$ s becomes much larger than the width of the flares ~ 40 s, and one finds that scenario 1 is inconsistent.[8]

To examine scenario 2, we consider an inhomogeneous shell (two components) expanding into the ISM. Corresponding to the major energy release from the central engine at the last moment, the inner edge of the shell with a width $\Delta_b/c \sim 40$ s is assumed to have an energy E_b larger than the energy $E_a \sim 10^{53}$ ergs in the preceding outer part with a width $\Delta_a/c \sim 200$ s. The Lorentz factors of the two components at the end of the internal shock phase are the same value of Γ. Both components should be in the thick-shell regime; otherwise the deceleration time of the shell becomes larger than the flare occurrence time ~ 200 s. The deceleration radius of the shell should be larger than the radius $R \sim \Delta_a^{1/4} l_a^{3/4}$ at which a reverse shock crosses the outer component where $l_a = l(E = E_a)$. The separation at the deceleration time between the gamma-ray front and the reference BM blast wave satisfies $S_B \gtrsim (\Delta_a/8)(E_a/E_b)$. The separation at that time between the gamma-ray front and the fireball is $S_F \sim \Delta_a + \Delta_b/4 \sim \Delta_a$, where we have assumed the fireball evolution $\Gamma \propto R^{-1/2}$ before the deceleration. Note that a broken power-law description of Γ around the deceleration radius is a good approximation in the thick-shell case. Then, we obtain $S_F/S_B \lesssim 8(E_b/E_a)$. The precursor discussion at the beginning of this section corresponds to the two component model with $E_a = 0$. We can show that the separation ratio at the deceleration time is $S_F/S_B \sim 8(\Delta_a/\Delta_b)$ in this

[8] In the afterglow modeling of this thin-shell case, measuring times from the GRB trigger does not cause an early steep decay, because the separation between the beginning of the prompt emission and the flare $\Delta t \sim 200$ s is smaller than the deceleration time $t_d \gtrsim 420$ s. As we have shown at the beginning of this section, a significant artificial steepening happens only when the ratio $\Delta t/t_d$ is larger than ~ 10.

case. Since replotting Figure 7 we have found that $\Delta_a/\Delta_b \gtrsim 10$ to produce an early steep decay, and in scenario 2 E_b should be at least 10 times larger than E_a. This requires a large energy budget for the central engine $E \gtrsim 10^{54}$ ergs. Even in the limit of $E_a/E_b = 0$, the small ratio $\Delta_a/\Delta_b \sim 200/40 = 5$ does not lead to a very steep decay of $\alpha \gtrsim 3$–5. Therefore, we conclude that even an inhomogeneous fireball cannot produce X-ray flares in early afterglow via external shock emission process.

5. CONCLUSIONS

We have studied the reference time t_0 for the afterglow modeling. Although measuring times from the beginning of the prompt emission (GRB trigger) might cause a slight overestimate of the early afterglow slope in the thick-shell case. This choice of t_0 gives a reasonable approximation, and it does not induce a very steep decay ($\alpha \sim 3$–5) like the early steep decay or X-ray flares in the canonical *Swift* X-ray light curve.

The leading model to explain the rapid decay and flares in early X-ray afterglow is the internal shock emission. A clear, testable prediction of this model is that the temporal decay index α of the tail part should be related to the spectral index β by an equation $\alpha = 2 + \beta$ (Kumar & Panaitescu 2000). When evaluating the emission decay $L \propto (t - t_0)^{-\alpha}$ in the internal shock model, an important difference is that the GRB trigger time is no longer special. The reference time t_0 should correspond to the onset of each particular spike in the prompt emission or in afterglow (Kobayashi et al. 1997; Zhang et al. 2006b; Nousek et al. 2006; Fan & Wei 2005). Every time the central engine is restarted to eject subshells, the reference time t_0 should be reset to the reactivation time of the engine. Although O'Brien et al. (2006) have found that α appears to be largely independent of β when the BAT trigger time is used as t_0, Liang et al. (2006) have shown that the relation $\alpha = 2 + \beta$ is more or less satisfied in most cases if t_0 is set near the beginning of rising segment of the last pulse of the prompt emission or a corresponding X-ray flare, and if the underlying forward shock emission component is subtracted. *Swift* observations support the internal shock model.

The self-consistent internal shock interpretation should be more favorable than the beginning-of-the-afterglow interpretation. The latter cannot explain multiple X-ray flares in a single event. Such behavior is observed in many *Swift* bursts (Burrows et al. 2005; Falcone et al. 2006; Romano et al. 2006; O'Brien et al. 2006). Usually X-ray flux already begins to decay before X-ray flares appear, and it suggests that the onset of afterglow is prior to the flares. If a large amount of energy is impulsively injected into a fireball during the deceleration, t_0 might be reset to the injection time. However, an afterglow baseline also should shift after a flare (energy injection). This clearly contradicts observations in which after a flare peak, afterglow decays back to its preflare flux level. We cannot explain X-ray flares by the shift of t_0 associated with large energy injections.

Swift discovered that a large fraction of X-ray afterglows have a slow decay phase, and it has been suggested that energy injection into a blast wave takes place several hundred seconds after the burst. This implies that right after the burst the kinetic energy of a blast wave is very low and in turn the efficiency of internal shock process is extremely high (Zhang et al. 2006b; Nousek et al. 2006; Ioka et al. 2006; Granot et al. 2006; Zhang et al.2006a; however, see also Fan & Piran 2006). The round-off forward shock peak in the thin-shell case might be a good candidate for the shallow decay phase. However, if we interpret the observed shallow decay as the round shape of the deceleration phase, the model light curve is shallower than some of the observed ones. This may be because the observed curve is the combination of this round phase and the rapid decay from the GRB tail emission (high latitude). Equalizing the deceleration time and the shallow phase timescale, we obtain the initial Lorentz factor $\Gamma_0 \sim 110\zeta^{3/8}E_{53}^{1/8}\rho_{1,-1}^{-1/8}t_{d,3}^{-3/8}$, where the time dilation effect is taken into account $\zeta = (1 + z)/3$.

For a wind environment, we can discuss the t_0 issue in a very similar way. The Lorentz factor of a shocked shell is constant in both of the thin and thick-shell cases during the shock crossing, while the BM blast wave decelerates as $\Gamma \propto R^{-1/2}$ (Kobayashi & Zhang 2003). The separations are comparable $S_F \sim 2S_B$ at the deceleration time. Measuring times from the beginning of the prompt phase should be a good approximation for events in a wind environment also. Since most bursts in a wind environment fall in the thick-shell case (Kobayashi et al. 2004), and since the deceleration time is comparable to GRB duration in the thick-shell case, another process (e.g., refreshed shocks) rather than the afterglow peak is necessary to explain the shallow decay phase.

We thank Luigi Piro for useful discussion. This work is supported by NASA NNG05GB67G and NNG06GH62G.

REFERENCES

Barthelmy, S. D., et al. 2005, Nature, 438, 994
Blandford, R. D., & McKee, C. F. 1976, Phys. Fluids, 19, 1130
Burrows, D., et al. 2005, Science, 309, 1833
Chincarini, G., et al. 2005, ApJ, submitted (astro-ph/0506453)
Falcone, A. D., et al. 2006, ApJ, 641, 1010
Fan, Y., & Piran, T. 2006, MNRAS, 369, 197
Fan, Y., & Wei, D. M. 2005, MNRAS, 364, L42
Granot, J., Königl, A., & Piran, T. 2006, MNRAS, 370, 1946
Ioka, K., Kobayashi, S., & Zhang, B. 2005, ApJ, 631, 429
Ioka, K., Toma, K., Yamazaki, R., & Nakamura, T. 2006, A&A, 458, 7
Kobayashi, S. 2000, ApJ, 545, 807
Kobayashi, S., Mészáros, P., & Zhang, B. 2004, ApJ, 601, L13
Kobayashi, S., Piran, T., & Sari, R. 1997, ApJ, 490, 92
———. 1999, ApJ, 513, 669
Kobayashi, S., & Sari, R. 2000, ApJ, 542, 819
Kobayashi, S., & Zhang, B. 2003, ApJ, 597, 455
Kumar, P., & Panaitescu, A. 2000, ApJ, 541, L51
Lazzati, D., & Begelman, M. C. 2006, ApJ, 641, 972
Lazzati, D., Ramirez-Ruiz, E., & Ghisellini, G. 2001, A&A, 379, L39
Liang, E. W., et al. 2006, ApJ, 646, 351
Martí, J. M., & Müller, E. 1999, Living Rev. Relativity, 2, 3
Nakar, E., & Piran, T. 2004, MNRAS, 353, 647
Nousek, J. A., et al. 2006, ApJ, 642, 389
O'Brien, P. T., et al. 2006, ApJ, 647, 1213
Piro, L., et al. 2005, ApJ, 623, 314
Quimby, R. M., et al. 2006, ApJ, 640, 402
Romano, P., et al. 2006, A&A, 450, 59
Sari, R. 1997, ApJ, 489, L37
Sari, R., & Piran, T. 1995, ApJ, 455, L143
Sari, R., Piran, T., & Narayan, R. 1998, ApJ, 497, L17
Tagliaferri, G., et al. 2005, Nature, 436, 985
Waxman, E. 1997, ApJ, 491, L19
Zhang, B., et al. 2007, ApJ, in press (astro-ph/061077)
Zhang, B., et al. 2006b, ApJ, 642, 354